



## Article

# Spatiotemporal Variations of Vegetation and Its Response to Climate Change and Human Activities in Arid Areas—A Case Study of the Shule River Basin, Northwestern China

Xiaorui He <sup>1,2,\*</sup> , Luqing Zhang <sup>2</sup>, Yuehan Lu <sup>3</sup>  and Linghuan Chai <sup>1</sup><sup>1</sup> College of Civil Engineering and Architecture, Quzhou University, Quzhou 324000, China<sup>2</sup> Institute of Geology and Geophysics, Chinese Academy of Sciences, Beijing 100045, China; zhangluqing@mail.iggcas.ac.cn<sup>3</sup> Department of Geological Sciences, University of Alabama, Tuscaloosa, AL 35487, USA; yuehan.lu@ua.edu

\* Correspondence: hexiaorui@mail.hfut.edu.cn

**Abstract:** The Shule River Basin (SRB) is a typical arid area in northwest China with a fragile ecology. Understanding vegetation dynamics and its response to climate change and human activities provides essential ecological and environmental resource management information. This study extracted fractional vegetation coverage (FVC) data from 2000 to 2019 using the Google Earth Engine platform and Landsat satellite images, employing trend analysis and other methods to examine spatiotemporal changes in vegetation in the SRB. Additionally, we used partial correlation and residual analyses to explore the response of FVC to climate change and human activities. The main results were: (1) The regional average FVC in the SRB showed a significant upward trend from 2000 to 2019, increasing by  $1.3 \times 10^{-3} \text{ a}^{-1}$ . The area within 1 km of roads experienced a higher increase of  $3 \times 10^{-3} \text{ a}^{-1}$ , while the roadless areas experienced a lower increase of  $1.1 \times 10^{-3} \text{ a}^{-1}$ . The FVC spatial heterogeneity in the SRB is significant. (2) Partial correlation analysis shows that the FVC correlates positively with precipitation and surface water area, with correlation coefficients of 0.575 and 0.744, respectively. A weak negative correlation exists between the FVC and land surface temperature (LST). FVC changes are more influenced by precipitation than by LST. (3) The contributions of climate change to vegetation recovery are increasing. Human activities, particularly agricultural practices, infrastructure development, and the conversion of farmland to grassland, significantly influence vegetation changes in densely populated areas. (4) The area changes of different land types are closely related to climate factors and human activities. Increased construction, agricultural activity, and converting farmland back to grassland have led to an increase in the area proportions of “impervious surfaces”, “cropland”, and “grassland”. Climate changes, such as increased rainfall, have resulted in larger areas of “wetlands” and “sparse vegetation”. These results provide valuable information for ecosystem restoration and environmental protection in the SRB.

**Keywords:** arid environment; ecosystem restoration; fractional vegetation coverage; spatiotemporal analysis



**Citation:** He, X.; Zhang, L.; Lu, Y.; Chai, L. Spatiotemporal Variations of Vegetation and Its Response to Climate Change and Human Activities in Arid Areas—A Case Study of the Shule River Basin, Northwestern China. *Forests* **2024**, *15*, 1147. <https://doi.org/10.3390/f15071147>

Academic Editor: Nikolay S. Strigul

Received: 20 May 2024

Revised: 27 June 2024

Accepted: 30 June 2024

Published: 1 July 2024



**Copyright:** © 2024 by the authors. Licensee MDPI, Basel, Switzerland. This article is an open access article distributed under the terms and conditions of the Creative Commons Attribution (CC BY) license (<https://creativecommons.org/licenses/by/4.0/>).

## 1. Introduction

Vegetation is essential to terrestrial ecosystems, playing a critical role in ecosystem functioning and delivering key ecosystem services [1]. In the arid regions of northwest China, the fragile natural environment, coupled with the unsustainable development and exploitation of natural resources, has intensified ecological issues such as vegetation degradation and desertification [2,3]. Understanding how vegetation dynamics respond to climate change and human activities is a key research focus due to its crucial role and ever-changing nature [4]. However, recent studies have suggested that in ecologically vulnerable regions, inappropriate ecological restoration measures that fail to account for local climate factors have led to low survival rates of restored plants and even the

deterioration of local ecosystems [5–8]. Therefore, examining the spatial and temporal variations of vegetation greenness on a regional scale is crucial for ecological protection and sustainable development [9].

The succession of vegetation cover is influenced by the climate, natural environmental factors, and human activities [10–25]. In recent years, various human activities, such as urban expansion and resource development, have profoundly disturbed the regional ecological environment, posing a serious threat to its stability [26–29]. Previous studies have extensively investigated the spatiotemporal evolution of vegetation cover in the arid regions of northwest China [30,31], driven by both climate change and human activities [32–34]. Techniques like geographic information systems (GIS) and remote sensing (RS) have been utilized to study the dynamic evolution of vegetation [26]. Remote sensing technology, particularly the use of satellite-derived indices like the normalized difference vegetation index (NDVI), has proven to be an effective tool for monitoring vegetation changes over large areas and extended periods [26]. Previous studies have utilized NDVI data to analyze vegetation trends and their relationship with climatic factors in various regions. For example, a fractional vegetation coverage (FVC) time series analysis from 1986 to 2021 in the Qilian Mountain National Nature Reserve revealed that climate variability and human activities contributed significantly to vegetation variations [35]. Similarly, the Qinghai–Tibet Plateau’s vegetation changes have been attributed to human activities and climate variability [34,36,37]. Meanwhile, extreme weather and land desertification caused by climate change have heightened awareness among humans about the crisis of ecological environment deterioration [38]. Moreover, recent advancements in remote sensing methodologies have further enhanced our ability to classify and monitor plant ecological communities [39].

The Hexi Corridor, situated in northwest China, is a typical representation of an arid region, with the Shule River Basin (SRB) being one of its primary inland river basins. The SRB, characterized by a landscape of mountains, oases, and deserts, experiences limited rainfall, high evaporation rates, and uneven water distribution, making its ecosystem particularly delicate and vulnerable. It is also among the most susceptible regions to the impacts of climate change globally [40]. The overexploitation of water resources has exacerbated ecological issues in the basin, including sparse vegetation, grassland degradation, soil salinization, wetland reduction, and desertification [41]. These challenges are anticipated to influence future development planning in the area significantly. Therefore, studying the spatiotemporal dynamics of vegetation in the SRB and its responses to climate change and human activities holds scientific significance and crucial economic and social implications. Despite previous studies focusing on the impact of natural and social factors on the SRB, few have conducted large-scale and long-term dynamic analyses of the vegetation coverage. The ecological fragility of the basin, exacerbated by climate variability and human activities, poses significant challenges. Extreme events such as precipitation, drought, and human activities like farming, industry, and construction further destabilize vegetation coverage [35,42,43]. Monitoring vegetation growth and change is essential for promoting ecological protection and sustainable economic development in the region. It is imperative to undertake dynamic research on FVC in the basin. The FVC quantifies the surface vegetation status and is crucial for assessing vegetation change, soil and water conservation, and climate impacts.

In this study, we assess the impact of climate change and human activities on vegetation change in the Shule River Basin (SRB). Using the Google Earth Engine (GEE) platform, we extracted fractional vegetation coverage (FVC) time series data from 2000 to 2019 and conducted spatiotemporal analyses to monitor vegetation coverage changes. The objectives are to monitor temporal and periodic changes in vegetation coverage and analyze the spatial distribution to gain insights into the ecological consequences of climate variations and human activities, especially in arid ecotone zones. The main goals of this study are: (1) to analyze the temporal and spatial dynamic trends of vegetation in the SRB; (2) to identify the response mechanisms of vegetation changes in the SRB

to human activities, such as road construction; (3) to determine the dominant climate factors affecting vegetation change in the SRB; and (4) to identify land cover dynamics and their responses to climate change and human activities.

## 2. Materials and Methods

### 2.1. Study Area

The Shule River Basin (SRB) is situated in the Gansu Province, China, spanning from a longitude of  $92^{\circ}11'$  E to  $98^{\circ}30'$  E and a latitude of  $38^{\circ}0'$  N to  $42^{\circ}48'$  N. It lies at the westernmost edge of the Hexi Corridor. This region is a transition zone between the Qinghai-Tibet Plateau and the Alashan Plateau of Inner Mongolia, forming an integral part of the historic “Silk Road”. Spanning an area of approximately 100,000 km<sup>2</sup>, the Shule River is one of the three major inland rivers in the Hexi Corridor (Figure 1a). The SRB experiences a temperate, arid climate with ample and intense solar radiation. The annual average temperature ranges from 7 to 9 °C. Despite its limited annual average rainfall of less than 60 mm, the region witnesses high evaporation rates ranging from 1500 to 3000 mm [44]. Altitudes in the study area vary significantly, ranging from 660 to 4545 m above sea level.

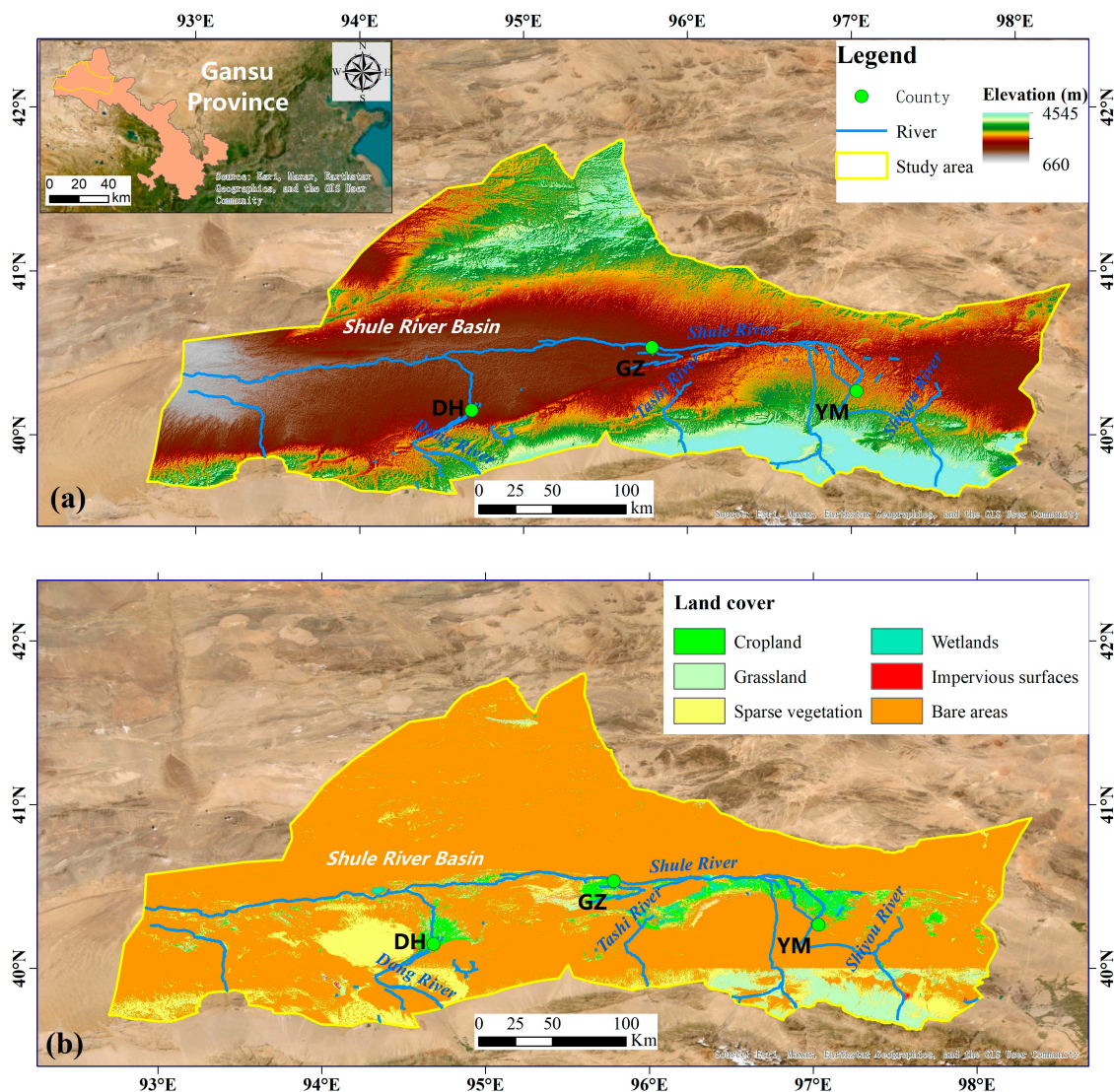


**Figure 1.** Overview of the study area. (a) The geographic location and terrain of the Shule River Basin, and (b) the land cover types of the Shule River Basin, including cropland, grassland, sparse vegetation, wetlands, impervious surfaces, and bare areas.

Surface water resources in the SRB are scarce. The land cover types in the SRB encompass a diverse range of ecosystems, including croplands, grasslands, sparse vegetation, wetlands, impervious surfaces, and bare areas (Figure 1b). Given its unique geographical and climatic features, as well as its historical significance along the Silk Road, the SRB presents an ideal study area for exploring vegetation dynamics influenced by climate change and human activities.

## 2.2. Datasets

### 2.2.1. Vegetation

The main dataset employed in this study comprises annual Fractional Vegetation Cover (FVC) data derived from annual Normalized Difference Vegetation Index (NDVI) data. The NDVI data were obtained from Landsat TM/OLI satellite data products, including Landsat 5 TM, Landsat 7 ETM, and Landsat 8 OLI, synthesized using the Google Earth Engine (GEE) platform (<https://developers.google.com/earth-engine> (accessed on 1 January 2023)). The data span from 2000 to 2019, with a spatial resolution of 30 m.

This approach ensures the comprehensive assessment of vegetation dynamics over the study period, allowing for detailed spatiotemporal analysis of vegetation changes in the SRB. The detailed calculation methodology will be elaborated on in Section 2.3.1.

### 2.2.2. Land Cover

The land cover data utilized in this study were sourced from the Global 30-m Land Cover Products with a Fine Classification System in 2020 (GLC\_FCS30-2020). This dataset provides comprehensive land cover information with an exemplary classification system derived from continuous time-series Landsat imagery on the GEE platform. The GLC\_FCS30-2020 dataset offers detailed and up-to-date land cover classification for the study area, enabling a precise analysis of land cover dynamics. The dataset covers various land cover types, including croplands, grasslands, sparse vegetation, wetlands, impervious surfaces, and bare areas. The land cover types in the study area are defined as follows: “Cropland” refers to land used for agricultural purposes, including mature, cultivated land, newly reclaimed land, fallow land, rotational rest land, and areas undergoing grassland rotation cropping, among others. “Grassland” encompasses various types of land predominantly covered by herbaceous plants, forming different grasslands. “Sparse vegetation” represents areas with limited vegetation cover, characterized by scattered vegetation patches. “Wetland” includes areas with high water saturation, such as marshes, swamps, and other waterlogged habitats. “Impervious surfaces” refer to urban and rural residential areas, industrial zones, mining sites, transportation infrastructure, and other human-built surfaces that prevent water infiltration. “Bare areas” denote areas devoid of vegetation cover, typically consisting of exposed soil, rock, or other non-vegetated surfaces.

These land cover categories provide valuable insights into the landscape composition and land use patterns within the study area, facilitating a comprehensive analysis of vegetation dynamics and ecosystem changes over time.

### 2.2.3. Precipitation

The precipitation data utilized in this study were obtained from the Climate Hazards Group InfraRed Precipitation with Station data (CHIRPS). CHIRPS is a long-term quasi-global rainfall dataset spanning over 30 years. It integrates high-resolution satellite imagery with in-situ station data to generate gridded rainfall time series, enabling trend analysis and seasonal drought monitoring [45]. The CHIRPS dataset provides reliable and spatially detailed information on precipitation patterns, making it suitable for analyzing temporal variations in rainfall. For this study, we extracted the annual mean precipitation data from 2000 to 2019 using the GEE platform. The precipitation data were resampled to 30-m resolution using the ArcGIS 10.8 software. Resampling the precipitation data to a finer resolution enhances its utility by capturing localized

variations in rainfall patterns and facilitating a more accurate analysis of its effects on vegetation dynamics. This high-resolution precipitation dataset is valuable input for assessing the relationship between precipitation variability and vegetation changes in the SRB over the study period.

#### 2.2.4. Land Surface Temperature

The Landsat series of satellites provides valuable data for monitoring the land surface temperature (LST), offering high spatial resolution and frequent revisit times. Researchers can obtain reliable and spatially detailed LST data for various applications, including climate studies, environmental monitoring, and land surface modeling [37]. The LST data used in this study were acquired from the GEE platform using open-source code designed explicitly for LST estimation from the Landsat series [46]. Accessing LST data through the GEE platform and utilizing open-source code for processing ensures transparency, reproducibility, and accessibility of the data, facilitating robust scientific analysis and the interpretation of land surface temperature dynamics in the SRB [47].

#### 2.2.5. Surface Water Area

The surface water data utilized in this study were obtained from the JRC Monthly Water History (v1.4) dataset. This dataset offers maps depicting the spatial distribution and temporal changes in surface water from 1984 to 2021. With a spatial resolution of 30 m, the JRC Monthly Water History dataset provides detailed information on the extent and dynamics of surface water bodies [37]. By analyzing the temporal distribution of surface water, we can assess changes in water bodies, including fluctuations in size, seasonal variations, and long-term trends in the SRB [48,49].

#### 2.2.6. DEM and Road

Digital Elevation Model (DEM) data were acquired from the Geospatial Data Cloud (<https://www.gscloud.cn/> (accessed on 1 January 2023)). The dataset is derived from the Advanced Spaceborne Thermal Emission and Reflection Radiometer (ASTER) Global Digital Elevation Model (GDEM) version 1 (V1). With a spatial resolution of 30 m by 30 m, the DEM dataset provides detailed information about the terrain elevation in the study area. Road data comes from the OpenStreetMap (OSM; [www.openstreetmap.org](http://www.openstreetmap.org) (accessed on 1 January 2023)).

### 2.3. Methods

Figure 2 shows the framework of this research. Firstly, the least squares method was adopted to detect vegetation trends from 2000 to 2019. Secondly, the relationship between climatic factors and the FVC was evaluated with partial correlation analysis. Finally, the residual analysis method was used to explore the main driving factor of spatial-temporal changes of FVC.

#### 2.3.1. Retrieval of FVC Time Series Data

Observations of the NDVI via remote sensing satellites are susceptible to various factors that may affect data quality. We used the annual maximum method to extract the NDVI values for each year. This method selects the highest NDVI value within the year, which typically corresponds to the growing season when vegetation is most active. By focusing on the maximum NDVI, we effectively capture the growing season dynamics while reducing the influence of cloud cover and water vapor on the NDVI observations [50]. This method utilizes the following calculation formula:

$$\text{NDVI}_i = \max(\text{NDVI}_j), \quad (1)$$

where  $NDVI_i$  represents the NDVI value in the  $i$  th year,  $NDVI_j$  is the NDVI value in the  $j$  th month of the  $i$  th year, and  $j$  is valued in the range of 1–12. The NDVI value was calculated as specified in Equation (2):

$$NDVI = (NIR - R) / (NIR + R), \quad (2)$$

where NIR is the near-infrared band spectral reflectance, and R is the red band spectral reflectance.

The NDVI is commonly used to derive the FVC [51]. The FVC can better measure surface vegetation conditions and environment changes [35]. The FVC was calculated using the Band Math calculation module of ENVI 5.0 after projection conversion and mosaicking as specified in Equation (3):

$$FVC = (NDVI - NDVI_{soil}) / (NDVI_{veg} - NDVI_{soil}), \quad (3)$$

where  $NDVI_{soil}$  and  $NDVI_{veg}$  represent the values of bare soil and full vegetation cover, respectively [35,52]. We use the NDVI values at the cumulative percentages of 0.5% and 99.5% as  $NDVI_{soil}$  and  $NDVI_{veg}$ , respectively. The detailed data are shown in Table 1.

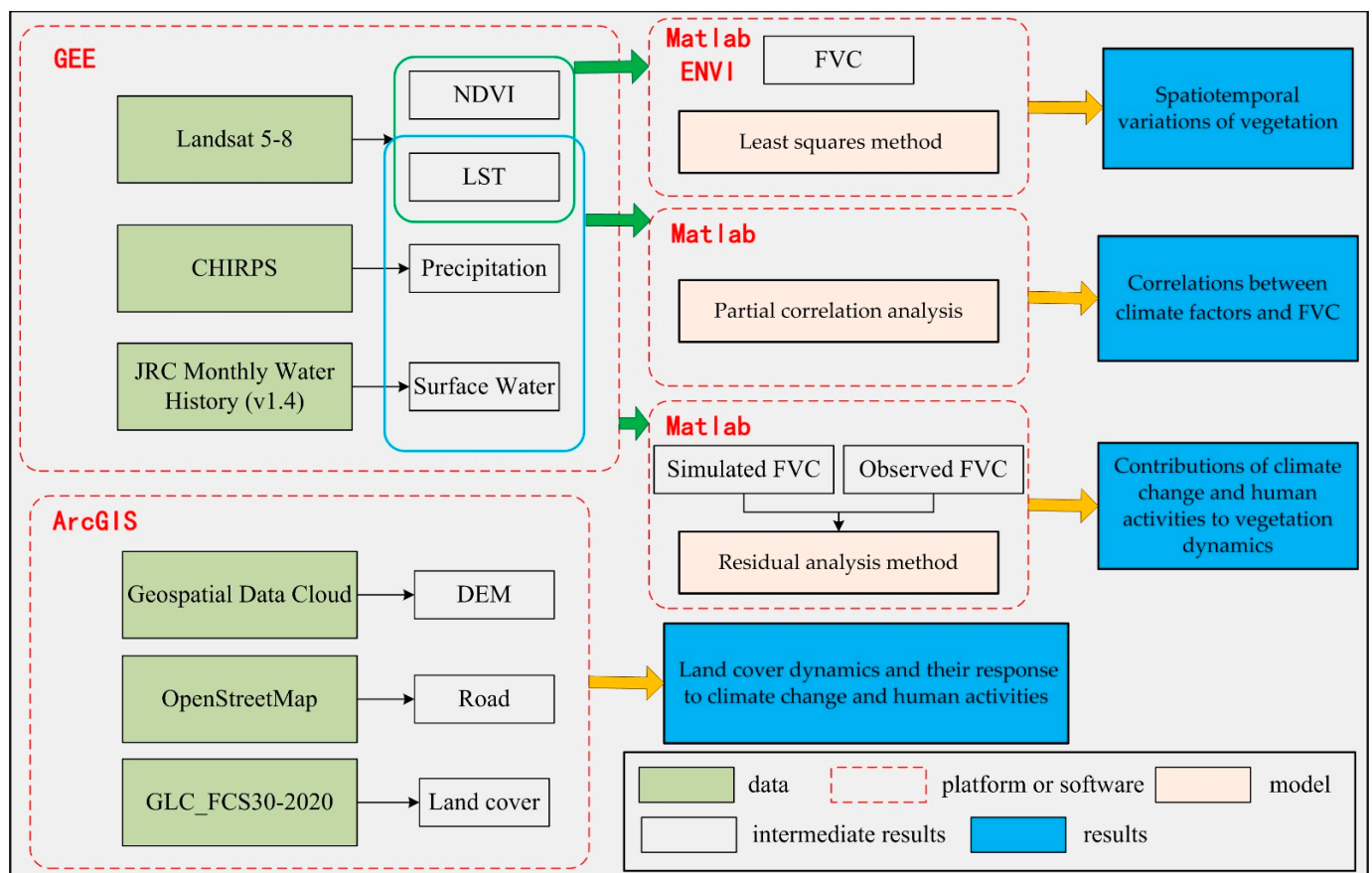


**Figure 2.** Framework of this research.

As suggested in a previous study, and in terms of the actual situation of the study area, the FVC was divided into five classes, namely extremely low [0–0.2], low [0.2–0.4], middle [0.4–0.6], middle high [0.6–0.8], and high [0.8–1.0] vegetation cover [35].

**Table 1.** The NDVI<sub>soil</sub> and NDVI<sub>veg</sub> value of the Shule River Basin.

Year	Minimum	Maximum	NDVI <sub>soil</sub> (0.5%)	NDVI <sub>veg</sub> (99.5%)
2000	−0.488	0.905	0.004	0.659
2001	−0.141	0.491	0.000	0.327
2002	−0.137	0.531	0.002	0.371
2003	−0.482	0.993	0.004	0.600
2004	−0.083	0.550	0.001	0.378
2005	−0.385	0.541	0.000	0.356
2006	−0.135	0.696	0.002	0.412
2007	−0.365	0.543	0.002	0.365
2008	−0.379	0.561	0.000	0.373
2009	−0.153	0.554	0.002	0.363
2010	−0.087	0.552	0.000	0.397
2011	−0.163	0.554	0.003	0.416
2012	−0.087	0.662	0.004	0.433
2013	−0.085	0.691	0.015	0.521
2014	−0.048	0.669	0.017	0.520
2015	0.001	0.686	0.017	0.516
2016	−0.009	0.680	0.015	0.501
2017	−0.055	0.680	0.015	0.507
2018	−0.035	0.677	0.018	0.520
2019	−0.106	0.671	0.016	0.513

### 2.3.2. Vegetation Trend Analysis

The linear trend of vegetation conditions was estimated using a simple linear regression in the study area from 2000 to 2019 and every five years separately (2000–2004, 2005–2009, 2010–2014, and 2015–2019) on a pixel scale. Trend analysis at the pixel scale can provide a more accurate reflection of vegetation spatiotemporal variations, which can better simulate areas where vegetation coverage is significantly improved and degraded [7,53]. The slope of the trend line in the multi-year regression equation for a single pixel represents the rate of variation, computed using the least squares method as follows [5,54–56]:

$$\text{Slope} = \frac{n \sum_{i=1}^n (i \times \text{FVC}_i) - \sum_{i=1}^n i \times \sum_{i=1}^n \text{FVC}_i}{n \sum_{i=1}^n i^2 - (\sum_{i=1}^n i)^2}, \quad (4)$$

where  $n$  is the sequence number of monitoring years (we divided the monitoring period (2000–2019) into four periods, where  $n$  is 5 for each period),  $\text{FVC}_i$  is the maximum value for the specific year, “Slope” is the slope of the linear regression, which represents the trend of FVC during each period. A positive slope (slope > 0.01) indicates an increased trend of FVC and vice versa. The significance of variation was determined using F-tests to calculate confidence levels ( $p < 0.05$ ) [57,58]. The vegetation trend analysis was performed in Matlab 2022b.

### 2.3.3. Partial Correlation Analysis

Partial correlation analysis describes the relationship between two variables while taking away the effects of another variable or several other variables [53]. We employed partial correlation analysis to evaluate the relationship between climatic factors (LST and precipitation) and FVC, which can exclude the confounding effects of other variables [59]. The calculation of the partial correlation coefficient can be expressed as follows:

$$r_{12.3} = \frac{r_{12} - r_{13}r_{23}}{\sqrt{(1 - r_{13}^2)(1 - r_{23}^2)}}, \quad (5)$$

where  $r_{12}$ ,  $r_{23}$ , and  $r_{13}$  refer to the correlation coefficients between  $Y$  and  $X_1$ ,  $Y$  and  $X_2$ , and  $X_1$  and  $X_2$ , respectively.  $r_{12.3}$  refers to the partial correlation coefficient between  $Y$  and  $X_1$

when the variable  $X_2$  is fixed [60]. Each partial correlation coefficient is tested using the  $t$ -test ( $p < 0.05$ ) [8].

#### 2.3.4. Calculating Contribution of Driving Factors to Variation in FVC

It is commonly assumed that the FVC is affected by the combined impact of human activities and climate variability [26,27,29,35,50,59,61–63]. The response of vegetation conditions to temperature and precipitation is often nonlinear [42]. The residual analysis method calculates the relative contributions of climate change and human activities to better attribute the observed vegetation changes to climate change and human activities [11,50].

First, a binary linear regression equation is constructed based on the LST and precipitation to predict the FVC only affected by climate change. Then, the predicted FVC value ( $FVC_c$ ) is calculated using the LST and precipitation data. Finally, the difference between the observed FVC and  $FVC_c$  is calculated and defined as the FVC residual, representing the variation rate of the contribution of unknown factors to FVC, which means the impact of human activities on FVC in this paper. The regression model for each pixel is as follows:

$$FVC_c = a \times LST + b \times Pre + c, \quad (6)$$

$$\varepsilon_i = FVC_i - FVC_{ci}, \quad (7)$$

where  $FVC_c$  is the simulated value of the multiple linear regression equation built based on climate factors;  $a$ ,  $b$ , and  $c$  are regression coefficients of the land surface temperature, precipitation, and a constant term, respectively;  $\varepsilon_i$  is the FVC residual between the observed FVC and the simulated FVC in the  $i$ th year;  $\varepsilon_i > 0$  and  $\varepsilon_i < 0$  separately indicate that human activities promote vegetation improvement and vegetation degradation.

This study used MATLAB software version R2020b under an academic license and ArcGIS software version 10.8 under an educational institution license.

### 3. Results

#### 3.1. Temporal Change of Vegetation

Figure 3 illustrates the changes in FVC area proportions from 2000 to 2019. The proportion of “extremely low cover” ranges from 92.13% to 95.61%, with an average of  $94.09\% \pm 1.03\%$ , and exhibited a decreasing trend with a slope of  $-0.163/a$  ( $R^2 = 0.87$ ). In contrast, the area proportions of “low coverage”, “middle coverage”, “middle-high coverage”, and “high coverage” show increasing trends, with slopes of  $0.080/a$  ( $R^2 = 0.68$ ),  $0.030/a$  ( $R^2 = 0.85$ ),  $0.023/a$  ( $R^2 = 0.84$ ) and  $0.030/a$  ( $R^2 = 0.74$ ), respectively. The results indicate an improvement in the ecological environment. Due to spatial heterogeneity, it is essential to analyze vegetation change patterns and their influencing factors.

Roads fragment landscapes and trigger human colonization and degradation of ecosystems. Ibsch et al. [64] defined the areas outside a 1-km buffer around all roads as “roadless areas”. According to this definition, we divided the study area into “road areas” and “roadless areas”. In “road areas”, vegetation changes were affected by both climate change and human activities. Therefore, we use  $V_{Climate+Human}$  to represent the average FVC in this area. Conversely, in the “roadless areas”, where human activity was minimal, vegetation changes were primarily driven by natural climate variations. Therefore, we use  $V_{Climate}$  to represent the average FVC in these regions. Finally,  $V_{All}$  represented the average FVC of the whole study area. Figure 4 depicts the trend of  $V_{Climate+Human}$ ,  $V_{All}$ , and  $V_{Climate}$ , showing significant increases ( $p < 0.05$ ) from 2000 to 2019, with slopes of  $1.3 \times 10^{-3} a^{-1}$ ,  $3 \times 10^{-3} a^{-1}$  and  $1.1 \times 10^{-3} a^{-1}$ , respectively.



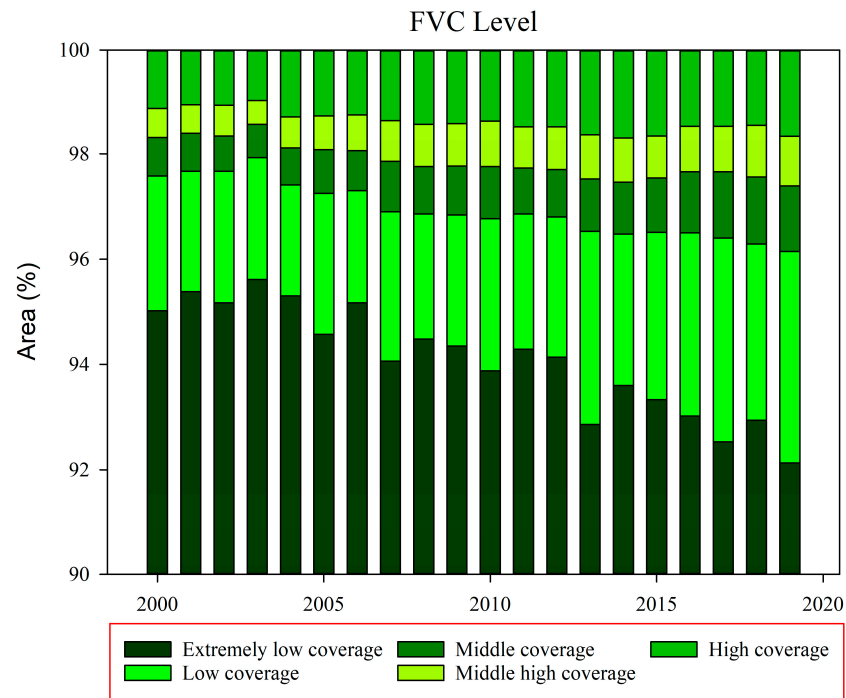


**Figure 3.** The temporal changes of vegetation coverage from 2000 to 2019 in SRB.

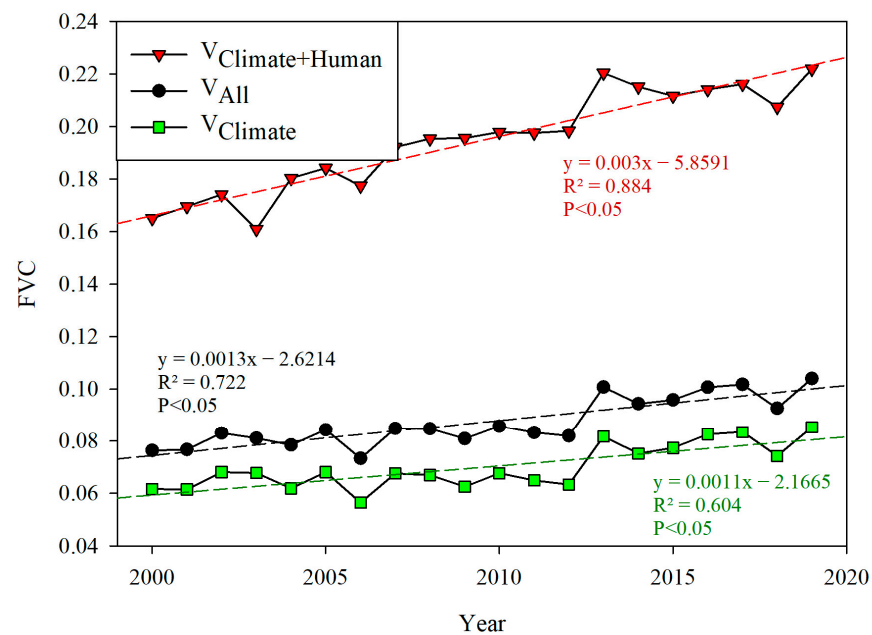


**Figure 4.** Dynamic changes of vegetation cover in “road areas” ( $V_{Climate+Human}$ ), “roadless areas” ( $V_{Climate}$ ), and the entire region ( $V_{All}$ ).

In arid regions, roads are generally constructed around oases, while “roadless areas” are primarily located in desert regions. Therefore, the mean FVC of “road areas” ( $V_{Climate+Human}$ ) tends to be higher than that of “roadless areas” ( $V_{Climate}$ ). The dynamic changes of  $V_{Climate}$  and  $V_{All}$  exhibit similar trends, while the dynamic changes of  $V_{Climate+Human}$  significantly declined in 2003, primarily due to human activities. Upon investigation, we discovered the construction of the Jia’an Highway from 2004 to 2006 in the study area, which significantly impacted the dynamic changes of vegetation (Figure 5).

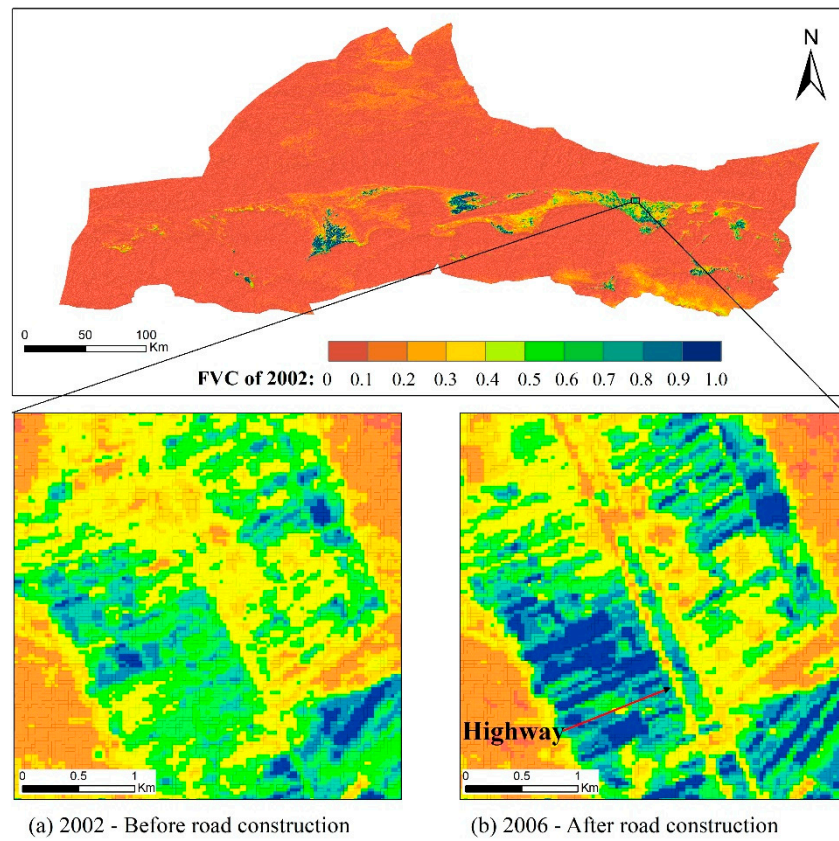
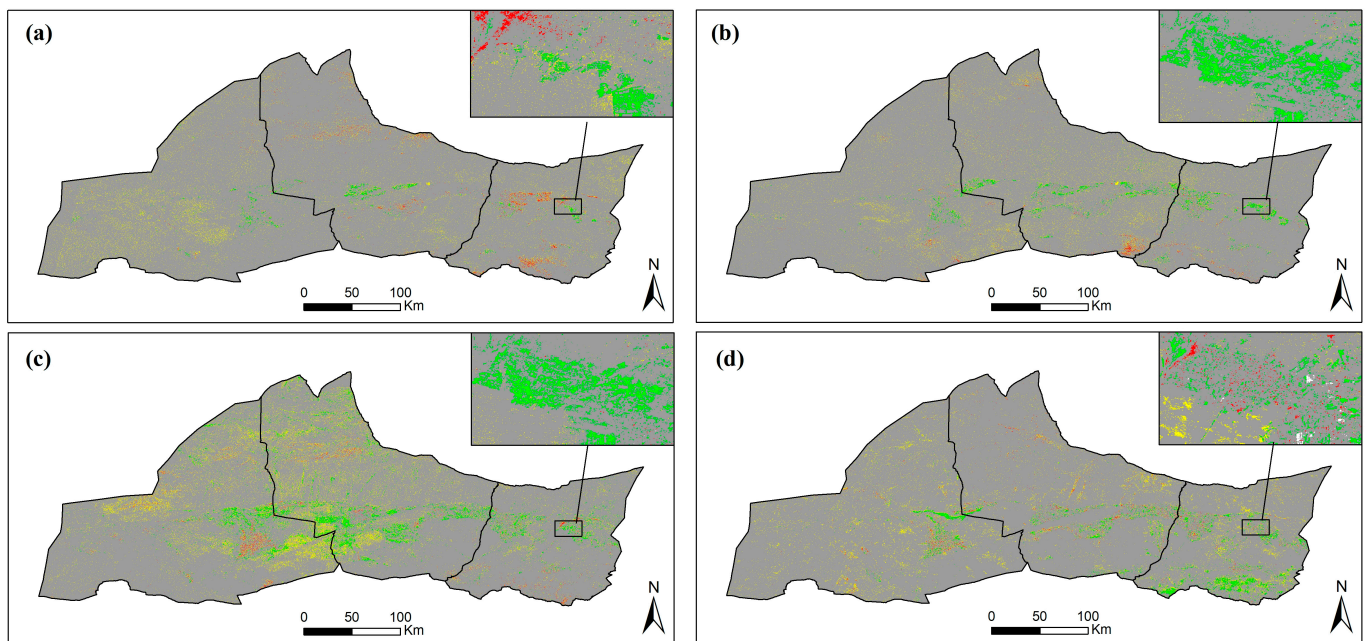


**Figure 5.** Vegetation changes caused by road construction.

3.2. Spatial Pattern of Vegetation Dynamics

Figure 6 depicts the trends of FVC in the entire SRB during the periods of 2000–2004, 2005–2009, 2010–2014, and 2015–2019. The findings are as follows:



The variation of vegetation coverage: ■ Significant decrease ■ Significant increase ■ Significant stable ■ Non-significant change

**Figure 6.** Spatial distribution of FVC and the significance of variations in FVC in the SRB in (a) 2000–2004, (b) 2005–2009, (c) 2010–2014, and (d) 2015–2019.

(a) From 2000 to 2004, the area exhibiting a significant increase in FVC accounted for 0.20%, primarily concentrated in the western part of Dunhuang and the eastern part of the Guazhou oasis (Table 2 and Figure 6). The area experiencing a significant decrease in vegetation cover accounted for 0.29% and was mainly distributed in the Yumen oasis and the desert zone in the northern part of the SRB.

**Table 2.** Summary of FVC trends.

Trend of FVC	$p$	Slope	Area (%)			
			2000–2004	2005–2009	2010–2014	2015–2019
Significantly increased	$p < 0.05$	slope $\geq 0.01$	0.20	0.38	0.89	0.68
Significantly decreased	$p < 0.05$	slope $\leq -0.01$	0.29	0.21	0.32	0.25
Significantly stable	$p < 0.05$	$-0.01 < \text{slope} < 0.01$	46.75	46.59	48.18	46.65
Non-significant change	$p \geq 0.05$	-	52.76	52.82	50.61	52.42

(b) During the period 2005–2009, the area witnessing a significant increase in vegetation cover expanded to 0.38%, predominantly observed in the oases of Dunhuang, Guazhou, and Yumen, as well as on both sides of the Shule River between the oases. Conversely, the area experiencing vegetation degradation accounted for 0.20% and was mainly distributed in the Qilian Mountains pre-mountainous zone southeast of the SRB.

(c) During 2010–2014, areas with a significant increase in vegetation cover expanded to 0.89%, while the proportion of regions witnessing a considerable decrease in vegetation cover accounted for 0.32% and was mainly concentrated in the oases in Dunhuang city.

(d) Finally, from 2015 to 2019, areas with a significant increase in vegetation cover extended to 0.68%, primarily concentrated in Dunhuang.

In summary, the dynamic changes in vegetation exhibit substantial spatial variability. While vegetation in the SRB generally shows an improving trend, the areas of change vary across different periods. Activities such as afforestation significantly increase FVC, whereas human activities like road construction notably reduce it.

### 3.3. Correlations between Climate Factors and FVC

Climate change and human activities influence the succession process of surface vegetation coverage. To comprehend how environmental factors impact vegetation variation in the study area, we gathered and calculated time series data of annual average precipitation, the highest LST, and the maximum area of surface water (Figures 7–9). Pearson correlation analysis was used to analyze the relationship between FVC and precipitation, LST, and surface water area (Table 3).

**Table 3.** The correlation coefficients of precipitation, LST, area of surface water, and FVC ( $V_{All}$ ).

	$V_{All}$	Precipitation	LST	Area of Surface Water
$V_{All}$	1	0.575	−0.107	0.744
Precipitation	0.575	1	−0.136	0.548
LST	−0.107	−0.136	0	0.030
Area of surface water	0.744	0.548	0.030	0

The FVC demonstrates a positive correlation with the annual average precipitation (Figure 7), with correlation coefficients of 0.575 (Figure 7 and Table 3). The FVC also positively correlates with the surface water area, with correlation coefficients of 0.744 (Figure 9 and Table 3). Meanwhile, precipitation and the area of surface water also exhibit a positive relationship, with a correlation coefficient of 0.548. Results suggest that precipitation promotes the increase of area of surface water and vegetation growth, with higher humidity associated with better vegetation growth.

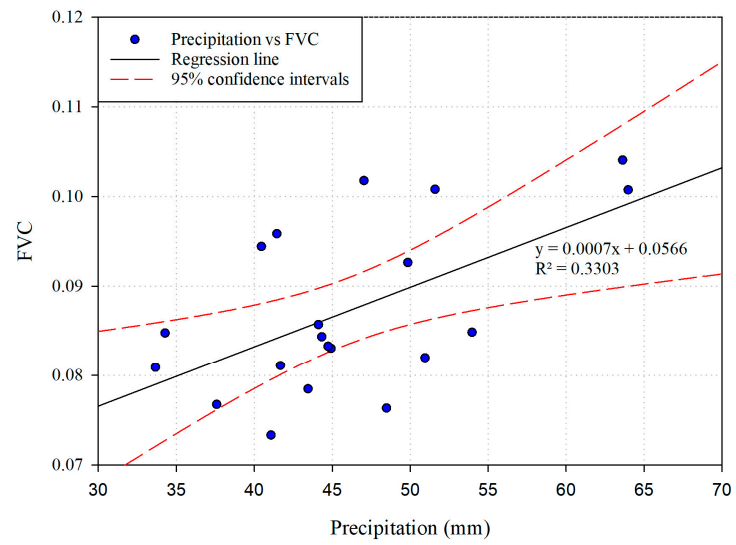


Figure 7. The relationship between precipitation and FVC.

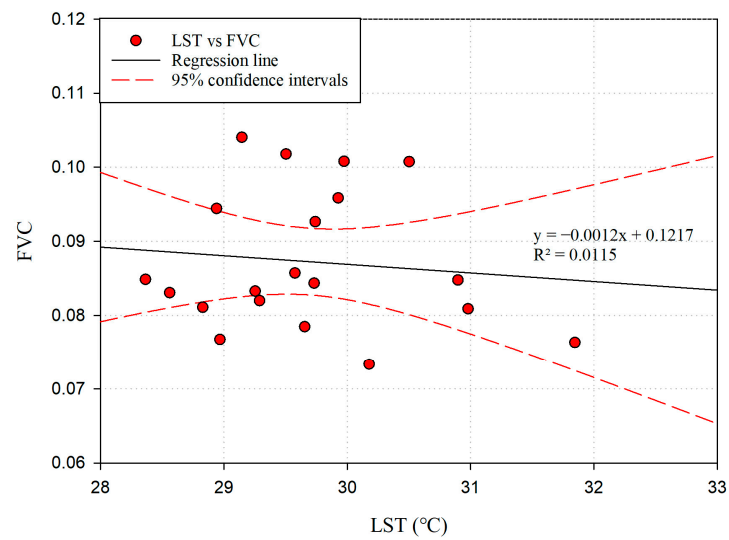


Figure 8. The relationship between LST and FVC.

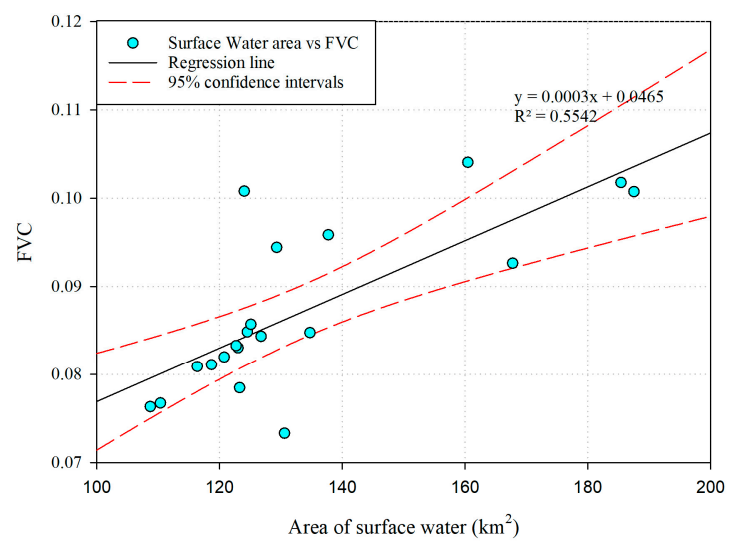
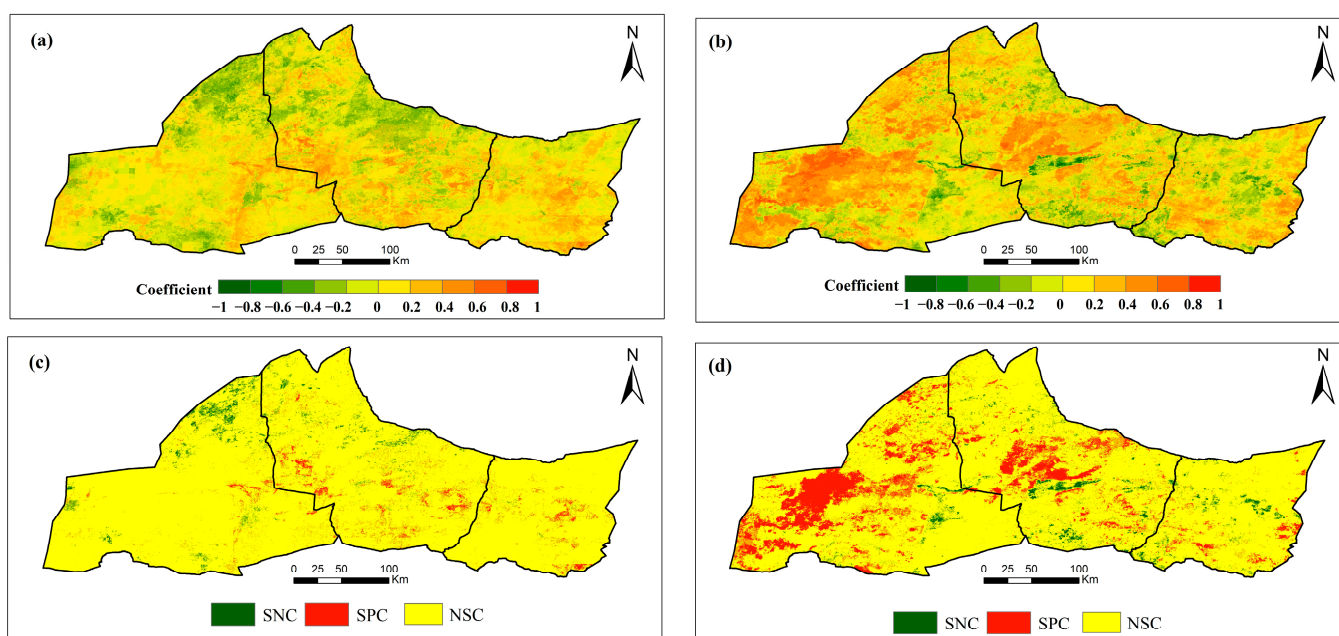


Figure 9. The relationship between the FVC and the area of surface water.

A weak negative correlation exists between the FVC and LST (Figure 8 and Table 3), with correlation coefficients of  $-0.107$ . In arid and semiarid areas, water is crucial for vegetation growth; hence, elevated temperatures may lead to increased evaporation, reduced water supply, exacerbated drought stress, and vegetation degradation [65]. Consequently, areas with higher LSTs exhibit poorer vegetation development. In recent years, northern desertification areas in China have generally witnessed rising temperatures and increased precipitation, leading to extended plant growth periods and enhanced vegetation growth.

Figure 10 illustrates the spatial distribution of the partial correlation coefficient between the FVC and climate factors. The partial correlation between FVC and precipitation shows the area of significant positive correlation (SPC) covering approximately 1.47% of the total area, primarily distributed in the middle of the SRB (Figure 10a,c). The area of SPC between the FVC and LST is mainly concentrated in the eastern and middle regions of the SRB and covers 7.64% of the total area (Figure 10b,d).



**Figure 10.** Partial correlation coefficient between FVC and climate. (a) FVC and precipitation (Pre) partial correlation. (b) FVC and LST partial correlation. (c) The relationship between FVC and precipitation. Significant negative correlation (SNC), significant positive correlation (SPC), and non-significant correlation (NSC). (d) The relationship between FVC and LST.

#### 4. Discussion

##### 4.1. Contributions of Climate Change and Human Activities to Vegetation Dynamics

Quantifying the relative contributions of human activities and climate factors to vegetation dynamics is crucial for understanding and addressing climate change impacts [65]. In this study, we quantified the spatiotemporal variations of FVC in the SRB from 2000 to 2019 and determined the contributions of climate change and human activities to vegetation dynamics.

Climate change, including factors like precipitation, temperature, and solar radiation, significantly influences vegetation dynamics in the SRB [26,27,29,66,67]. Previous research has highlighted the importance of these climate factors in affecting vegetation productivity, with precipitation generally promoting vegetation growth in arid and semiarid regions. At the same time, higher temperatures can inhibit it [35,38,68,69]. However, the impact of climate factors on FVC exhibits spatial heterogeneity across the study area.

Figure 11 illustrates the relative contributions of climate change and human activities to the increasing trend of FVC in the SRB from 2000 to 2019. Table 4 denotes the area proportion of the contribution of climate change and human activities to FVC increase. Climate change contributed to 17.47%, 25.48%, 28.31%, and 30.81% of the total area during 2000–2004, 2005–2009, 2010–2014, and 2015–2019, respectively. Human activities contributed to 24.14%, 30.45%, 25.69%, and 26.80% during the same periods.

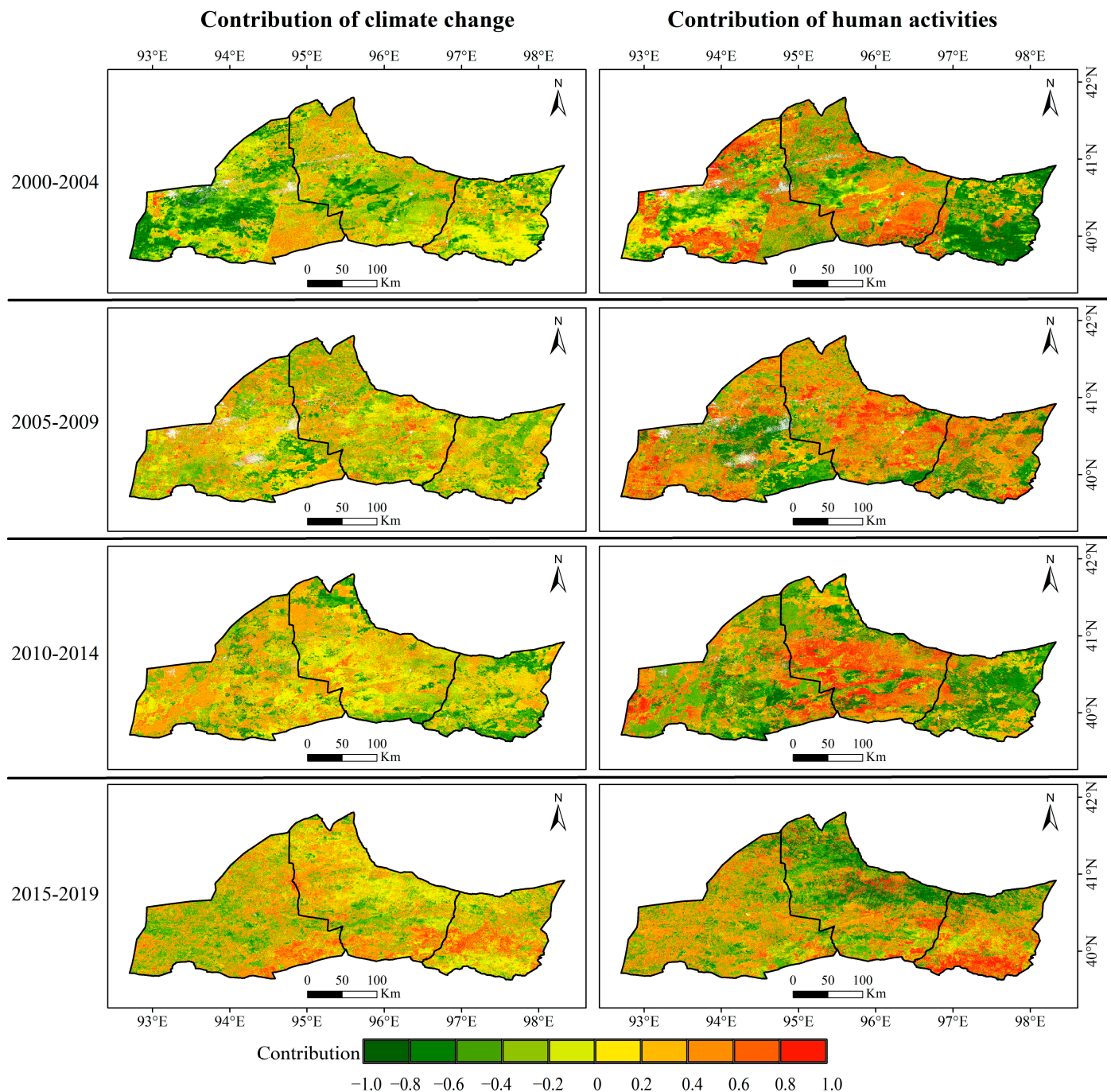


**Figure 11.** Contribution of climate change and human activities to annual variation in FVC from 2000 to 2019 in the SRB.

**Table 4.** The area proportion of the contribution of climate change and human activities to FVC increase.

	2000–2004	2005–2009	2010–2014	2015–2019
The contribution of climate change	17.47%	25.48%	28.31%	30.81%
The contribution of human activities	24.14%	30.45%	25.69%	26.80%

The results show that climate change is contributing to vegetation recovery. The areas with a positive contribution of human activities to FVC increase were mainly concentrated in the middle part of the SRB, where agricultural areas are prevalent. This reflects the significant impact of human activities on vegetation growth in more populated regions.

These findings underscore the complex interplay between climate change and human activities in shaping vegetation dynamics. While climate change emerges as a primary driver of vegetation recovery, human activities dominate densely populated areas, highlighting the need for targeted strategies to mitigate anthropogenic impacts on ecosystems while adapting to changing climatic conditions.

#### 4.2. Land Cover Dynamics and Their Response to Climate Change and Human Activities

Understanding the dynamic changes in land cover types is essential for comprehending the environmental changes driven by human activities and climate change. Variations in meteorological conditions, topography, and soil moisture across different land cover types significantly influence vegetation dynamics [70].

The relationship between the FVC and land cover types, as summarized in Table 5, underscores the complex interplay between vegetation dynamics and environmental factors. By analyzing the spatiotemporal changes in land cover types and their corresponding FVC proportions, we can gain insights into the responses of different ecosystems to human-induced and natural environmental changes.

**Table 5.** The relationship between FVC and land cover types.

Land Cover Types	FVC (%)									
	[0, 0.1]	(0.1, 0.2]	(0.2, 0.3]	(0.3, 0.4]	(0.4, 0.5]	(0.5, 0.6]	(0.6, 0.7]	(0.7, 0.8]	(0.8, 0.9]	(0.9, 1.0]
Cropland	0.01	3.32	19.03	31.73	46.81	56.59	68.38	79.62	83.80	83.47
Grassland	0.45	28.61	41.77	38.87	32.75	31.51	26.88	13.58	14.08	13.70
Sparse vegetation	8.05	23.67	23.30	11.32	6.59	2.25	1.19	1.89	0.00	0.47
Wetlands	0.17	0.81	10.60	15.87	10.77	4.18	1.19	1.13	1.76	0.00
Impervious surfaces	0.01	0.36	0.63	1.48	1.54	5.47	1.98	3.77	0.35	1.06
Bare areas	91.31	43.23	4.67	0.74	1.54	0.00	0.40	0.00	0.00	1.30

The area proportion of different land cover types can be estimated based on the proportion of land cover types in the FVC interval. Figure 12 illustrates the trends in various land cover types over the study period.

The area proportion of “bare areas” decreased from 84.401% in 2000 to 77.548% in 2019, a decrease of 6.853%, with an average annual decrease of about 0.307%. The results show that the area of bare land in the region has decreased, and the land cover type has changed significantly.

The area proportion of “grassland” ranges from 3.392% to 6.827%, averaging  $4.642 \pm 1.070\%$ . “Grassland” shows an increasing trend over time, with an increase rate of 0.145% per year. “Grassland” covers all types of land covered mainly by herbaceous plants. The increase in grassland area may be caused by the combined effects of climate change and human activities, such as returning farmland to grassland [71,72].

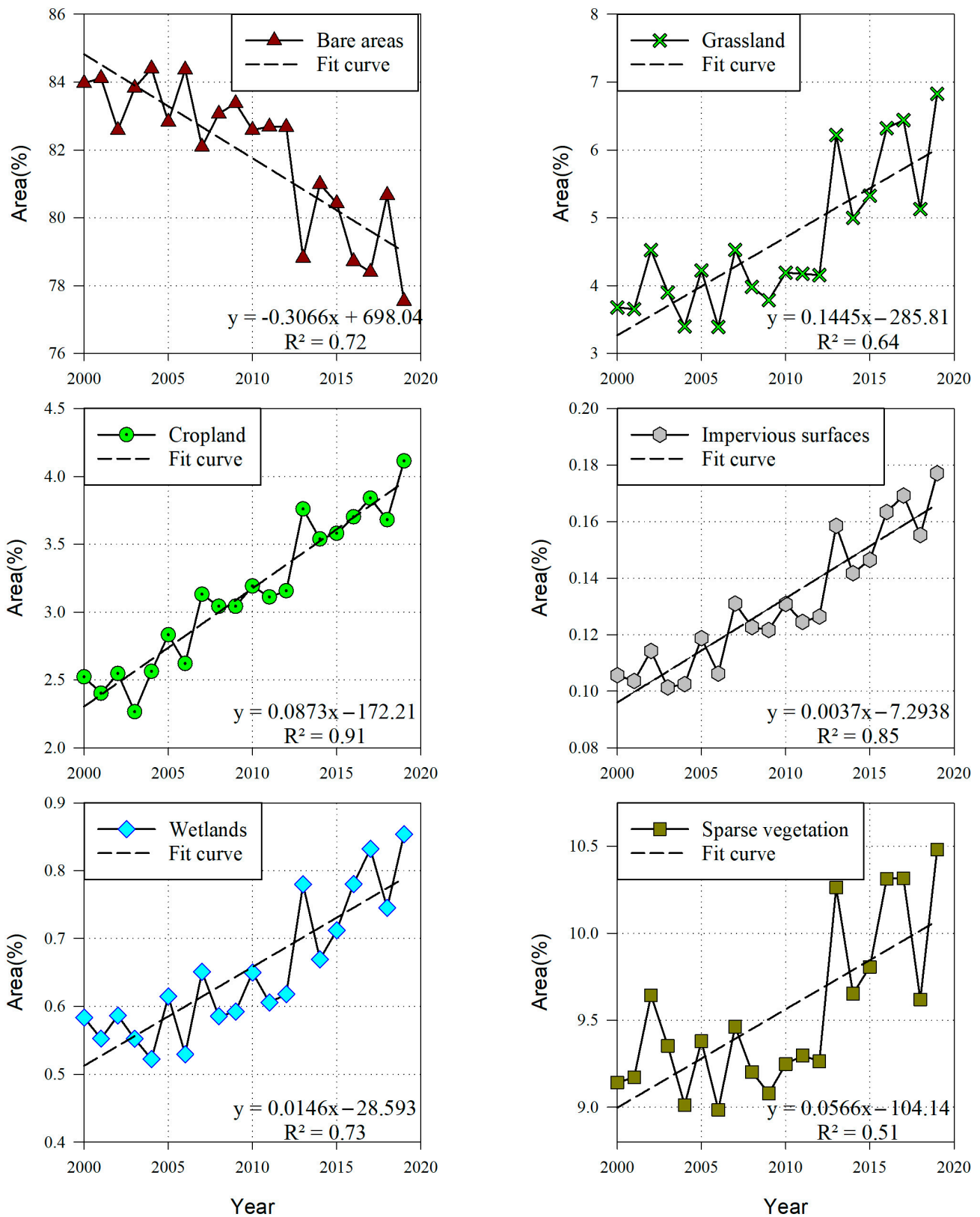


**Figure 12.** The area proportions of different land cover types from 2000 to 2019 in the SRB.

The area proportion of “cropland” ranges from 2.264% to 4.113%, with an average of  $3.132 \pm 0.540\%$ . The area of “cropland” is increasing at a rate of 0.087% per year, reflecting the expansion of agricultural activities.



Impervious surfaces are usually covered by anthropogenic materials that prevent water from penetrating into the soil [73]. The area proportion of “impervious surfaces” ranges from 0.101% to 0.177%, with an average of  $0.024 \pm 0.001\%$ . The rise in “impervious surfaces” highlights the ongoing urbanization and infrastructure development.

“Wetlands” include areas of high water saturation, such as marshes and other habitats, that are of great ecological importance. The area proportion of “wetlands” ranges from 0.522% to 0.854%, with an average of  $0.651 \pm 0.101\%$ . The area of “wetlands” increases at a rate of about 0.015% per year, reflecting the improvement of the ecological environment. The area proportion of “sparse vegetation” ranges from 8.985% to 10.482%, with an average of  $9.535 \pm 0.470\%$ . The proportion fluctuates greatly, with an  $R^2$  of 0.51.

The results of the analysis reflect the impact of human activities and climate change on land cover types. Activities such as construction, increased agricultural activity, and converting farmland back to grassland have led to an increase in the area proportions of “impervious surfaces”, “cropland”, and “grassland”. Climate changes, such as increased rainfall, have resulted in larger areas of “wetland” and “sparse vegetation”. Overall, under the influence of climate change and human activities, the proportion of “bare areas” has decreased, while vegetation cover and ecological conditions have shown positive development trends.

## 5. Conclusions

This study provides comprehensive insights into vegetation dynamics in the SRB from 2000 to 2019, shedding light on the impacts of climate change and human activities on ecosystem dynamics. The main results were as follows:

(1) This study reveals a significant upward trend in regional average FVC within the SRB from 2000 to 2019, with an increase of  $1.3 \times 10^{-3} \text{ a}^{-1}$ . Notably, areas proximal to roads experienced a higher FVC increase of  $3 \times 10^{-3} \text{ a}^{-1}$ , while roadless areas experienced a comparatively lower increase of  $1.1 \times 10^{-3} \text{ a}^{-1}$ . Additionally, road construction activities during 2004–2006 led to a notable reduction in FVC within a 200-m buffer of the roads.

(2) Spatial heterogeneity in FVC dynamics is pronounced within the SRB. While there is a general trend of improvement and increased vegetation cover, the magnitude and spatial distribution of these changes vary across different periods and locations. Afforestation initiatives significantly enhance FVC, whereas human activities like road construction have localized detrimental effects on vegetation.

(3) Partial correlation analysis highlights the influence of climatic factors on FVC dynamics within the SRB. The FVC shows positive correlations with precipitation (0.575) and surface water area (0.744), underscoring their pivotal roles in supporting vegetation growth. In contrast, a weak negative correlation is observed between the FVC and LST ( $-0.107$ ), indicating varying responses of vegetation to LST variations.

(4) Climate change has made a significant and growing contribution to vegetation restoration. However, human activities—especially agricultural practices, infrastructure development, and the conversion of farmland to grassland—play a vital role in vegetation changes in densely populated areas.

In summary, this study’s findings offer crucial insights into the complex interactions between environmental factors and human activities, providing valuable information for ecosystem restoration and environmental management initiatives in the SRB.

**Author Contributions:** Conceptualization, X.H.; Data curation, L.C.; Funding acquisition, X.H.; Investigation, X.H. and L.C.; Methodology, X.H.; Project administration, X.H.; Software, L.Z.; Supervision, L.Z. and Y.L.; Validation, X.H.; Visualization, X.H.; Writing—original draft, X.H.; Writing—review & editing, X.H., L.Z. and Y.L. All authors have read and agreed to the published version of the manuscript.

**Funding:** This research was funded by the Second Tibetan Plateau Scientific Expedition and Research Program (20190ZKK0904), the National Natural Science Foundation of China, grant number 42301098 and the Quzhou Science and Technology Plan program, grant numbers 2022K12, 2023K218.

**Data Availability Statement:** The original contributions presented in this study are included in the article; further inquiries can be directed to the corresponding author.

**Conflicts of Interest:** The authors declare no conflicts of interest.

## References

1. Lunetta, R.S.; Knight, J.F.; Ediriwickrema, J.; Lyon, J.G.; Worthy, L.D. Land-cover change detection using multi-temporal MODIS NDVI data. *Remote Sens. Environ.* **2006**, *105*, 142–154. [[CrossRef](#)]
2. Guan, Q.; Yang, L.; Guan, W.; Wang, F.; Liu, Z.; Xu, C. Assessing vegetation response to climatic variations and human activities: Spatiotemporal NDVI variations in the Hexi Corridor and surrounding areas from 2000 to 2010. *Theor. Appl. Climatol.* **2018**, *135*, 1179–1193. [[CrossRef](#)]
3. Wang, H.; Liu, G.; Li, Z.; Wang, P.; Wang, Z. Comparative Assessment of Vegetation Dynamics under the Influence of Climate Change and Human Activities in Five Ecologically Vulnerable Regions of China from 2000 to 2015. *Forests* **2019**, *10*, 317. [[CrossRef](#)]
4. Chen, Y.; Li, Z.; Fan, Y.; Wang, H.; Deng, H. Progress and prospects of climate change impacts on hydrology in the arid region of northwest China. *Environ. Res.* **2015**, *139*, 11–19. [[CrossRef](#)] [[PubMed](#)]
5. Fokeng, R.M.; Fogwe, Z.N. Landsat NDVI-based vegetation degradation dynamics and its response to rainfall variability and anthropogenic stressors in Southern Bui Plateau, Cameroon. *Geosyst. Geoenviron.* **2022**, *1*, 100075. [[CrossRef](#)]
6. Jiang, H.; Xu, X.; Guan, M.; Wang, L.; Huang, Y.; Jiang, Y. Determining the contributions of climate change and human activities to vegetation dynamics in agro-pastoral transitional zone of northern China from 2000 to 2015. *Sci. Total Environ.* **2020**, *718*, 134871. [[CrossRef](#)] [[PubMed](#)]
7. Liu, Y.; Zhang, Z.; Tong, L.; Khalifa, M.; Wang, Q.; Gang, C.; Wang, Z.; Li, J.; Sun, Z. Assessing the effects of climate variation and human activities on grassland degradation and restoration across the globe. *Ecol. Indic.* **2019**, *106*, 105504. [[CrossRef](#)]
8. Sun, B.; Li, Z.; Gao, W.; Zhang, Y.; Gao, Z.; Song, Z.; Qin, P.; Tian, X. Identification and assessment of the factors driving vegetation degradation/regeneration in drylands using synthetic high spatiotemporal remote sensing Data—A case study in Zhenglanqi, Inner Mongolia, China. *Ecol. Indic.* **2019**, *107*, 105614. [[CrossRef](#)]
9. Xue, X.; Wang, Z.; Hou, S. NDVI-Based Vegetation Dynamics and Response to Climate Changes and Human Activities in Guizhou Province, China. *Forests* **2023**, *14*, 753. [[CrossRef](#)]
10. Gao, W.; Zheng, C.; Liu, X.; Lu, Y.; Chen, Y.; Wei, Y.; Ma, Y. NDVI-based vegetation dynamics and their responses to climate change and human activities from 1982 to 2020: A case study in the Mu Us Sandy Land, China. *Ecol. Indic.* **2022**, *137*, 108745. [[CrossRef](#)]
11. Yu, M.; Song, S.; He, G.; Shi, Y. Vegetation Landscape Changes and Driving Factors of Typical Karst Region in the Anthropocene. *Remote Sens.* **2022**, *14*, 5391. [[CrossRef](#)]
12. He, J.; Shi, X.; Fu, Y. Identifying vegetation restoration effectiveness and driving factors on different micro-topographic types of hilly Loess Plateau: From the perspective of ecological resilience. *J. Environ. Manag.* **2021**, *289*, 112562. [[CrossRef](#)] [[PubMed](#)]
13. Zhang, X.; Jin, X. Vegetation dynamics and responses to climate change and anthropogenic activities in the Three-River Headwaters Region, China. *Ecol. Indic.* **2021**, *131*, 108223. [[CrossRef](#)]
14. Liu, N.; Ding, Y.; Peng, S. Temporal effects of climate on vegetation trigger the response biases of vegetation to human activities. *Glob. Ecol. Conserv.* **2021**, *31*, e01822. [[CrossRef](#)]
15. Teng, M.; Zeng, L.; Hu, W.; Wang, P.; Yan, Z.; He, W.; Zhang, Y.; Huang, Z.; Xiao, W. The impacts of climate changes and human activities on net primary productivity vary across an ecotone zone in Northwest China. *Sci. Total Environ.* **2020**, *714*, 136691. [[CrossRef](#)] [[PubMed](#)]
16. Zhao, S.; Pereira, P.; Wu, X.; Zhou, J.; Cao, J.; Zhang, W. Global karst vegetation regime and its response to climate change and human activities. *Ecol. Indic.* **2020**, *113*, 106208. [[CrossRef](#)]
17. Yin, L.; Dai, E.; Zheng, D.; Wang, Y.; Ma, L.; Tong, M. What drives the vegetation dynamics in the Hengduan Mountain region, southwest China: Climate change or human activity? *Ecol. Indic.* **2020**, *112*, 106013. [[CrossRef](#)]
18. Chen, T.; Bao, A.; Jiapaer, G.; Guo, H.; Zheng, G.; Jiang, L.; Chang, C.; Tuerhanjiang, L. Disentangling the relative impacts of climate change and human activities on arid and semiarid grasslands in Central Asia during 1982–2015. *Sci. Total Environ.* **2019**, *653*, 1311–1325. [[CrossRef](#)]
19. Meng, M.; Huang, N.; Wu, M.; Pei, J.; Wang, J.; Niu, Z. Vegetation change in response to climate factors and human activities on the Mongolian Plateau. *PeerJ* **2019**, *7*, e7735. [[CrossRef](#)]
20. Ma, Q.; Long, Y.; Jia, X.; Wang, H.; Li, Y. Vegetation response to climatic variation and human activities on the Ordos Plateau from 2000 to 2016. *Environ. Earth Sci.* **2019**, *78*, 709. [[CrossRef](#)]

21. Liu, R.; Xiao, L.; Liu, Z.; Dai, J. Quantifying the relative impacts of climate and human activities on vegetation changes at the regional scale. *Ecol. Indic.* **2018**, *93*, 91–99. [[CrossRef](#)]
22. Wu, Z.Y.; Saito, Y.; Zhao, D.N.; Zhou, J.Q.; Cao, Z.Y.; Li, S.J.; Shang, J.H.; Liang, Y.Y. Impact of human activities on subaqueous topographic change in Lingding Bay of the Pearl River estuary, China, during 1955–2013. *Sci. Rep.* **2016**, *6*, 37742. [[CrossRef](#)]
23. Zhang, J.; Niu, J.; Bao, T.; Buyantuyev, A.; Zhang, Q.; Dong, J.; Zhang, X. Human induced dryland degradation in Ordos Plateau, China, revealed by multilevel statistical modeling of normalized difference vegetation index and rainfall time-series. *J. Arid. Land.* **2013**, *6*, 219–229. [[CrossRef](#)]
24. Yang, T.; Zhang, Q.; Wang, W.; Yu, Z.; Chen, Y.D.; Lu, G.; Hao, Z.; Baron, A.; Zhao, C.; Chen, X.; et al. Review of Advances in Hydrologic Science in China in the Last Decades: Impact Study of Climate Change and Human Activities. *J. Hydrol. Eng.* **2013**, *18*, 1380–1384. [[CrossRef](#)]
25. Tu, X.; Zhang, Q.; Singh, V.P.; Chen, X.; Liu, C.-L.; Wang, S.-B. Space–time changes in hydrological processes in response to human activities and climatic change in the south China. *Stoch. Environ. Res. Risk Assess.* **2011**, *26*, 823–834. [[CrossRef](#)]
26. Liu, X.; Du, G.; Bi, H.; Li, Z.; Zhang, X. Normal Difference Vegetation Index Simulation and Driving Analysis of the Tibetan Plateau Based on Deep Learning Algorithms. *Forests* **2024**, *15*, 137. [[CrossRef](#)]
27. Li, G.; Liang, J.; Wang, S.; Zhou, M.; Sun, Y.; Wang, J.; Fan, J. Characteristics and Drivers of Vegetation Change in Xinjiang, 2000–2020. *Forests* **2024**, *15*, 231. [[CrossRef](#)]
28. Hou, X.; Zhang, B.; Chen, J.; Zhou, J.; He, Q.-Q.; Yu, H. Response of Vegetation Productivity to Greening and Drought in the Loess Plateau Based on VIs and SIF. *Forests* **2024**, *15*, 339. [[CrossRef](#)]
29. Zhang, Q.; Gu, L.; Liu, Y.; Zhang, Y. Spatio-Temporal Dynamics of Normalized Difference Vegetation Index and Its Response to Climate Change in Xinjiang, 2000–2022. *Forests* **2024**, *15*, 370. [[CrossRef](#)]
30. He, Q.; Yang, Q.; Jiang, S.; Zhan, C. A Comprehensive Analysis of Vegetation Dynamics and Their Response to Climate Change in the Loess Plateau: Insight from Long-Term kernel Normalized Difference Vegetation Index Data. *Forests* **2024**, *15*, 471. [[CrossRef](#)]
31. Shi, S.; Yu, J.; Wang, F.; Wang, P.; Zhang, Y.; Jin, K. Quantitative contributions of climate change and human activities to vegetation changes over multiple time scales on the Loess Plateau. *Sci. Total Environ.* **2021**, *755*, 142419. [[CrossRef](#)] [[PubMed](#)]
32. Li, B.; Chen, L.; Wang, Q.; Wang, P. Analysis of Linkage between Long-Term Morphological Spatial Pattern Analysis and Vegetation Carbon Storage of Forests in Hunan, China. *Forests* **2024**, *15*, 428. [[CrossRef](#)]
33. Araujo, H.F.P.; Canassa, N.F.; Machado, C.C.C.; Tabarelli, M. Human disturbance is the major driver of vegetation changes in the Caatinga dry forest region. *Sci. Rep.* **2023**, *13*, 18440. [[CrossRef](#)] [[PubMed](#)]
34. Zhu, B.; Zhang, Z.; Tian, J.; Kong, R.; Chen, X. Increasing Negative Impacts of Climatic Change and Anthropogenic Activities on Vegetation Variation on the Qinghai–Tibet Plateau during 1982–2019. *Remote Sens.* **2022**, *14*, 4735. [[CrossRef](#)]
35. Wang, X.; Zhang, X.; Li, W.; Cheng, X.; Zhou, Z.; Liu, Y.; Wu, X.; Hao, J.; Ling, Q.; Deng, L.; et al. Quantitative Analysis of Climate Variability and Human Activities on Vegetation Variations in the Qilian Mountain National Nature Reserve from 1986 to 2021. *Forests* **2023**, *14*, 2042. [[CrossRef](#)]
36. Ma, S.; Wang, L.-J.; Jiang, J.; Chu, L.; Zhang, J.-C. Threshold effect of ecosystem services in response to climate change and vegetation coverage change in the Qinghai-Tibet Plateau ecological shelter. *J. Clean. Prod.* **2021**, *318*, 128592. [[CrossRef](#)]
37. Luo, D.L.; Jin, H.J.; Bense, V.F. Ground surface temperature and the detection of permafrost in the rugged topography on NE Qinghai-Tibet Plateau. *Geoderma* **2019**, *333*, 57–68. [[CrossRef](#)]
38. Aizizi, Y.; Kasimu, A.; Liang, H.; Zhang, X.; Wei, B.; Zhao, Y.; Ainiwaer, M. Evaluation of Ecological Quality Status and Changing Trend in Arid Land Based on the Remote Sensing Ecological Index: A Case Study in Xinjiang, China. *Forests* **2023**, *14*, 1830. [[CrossRef](#)]
39. Sharma, R.C. Dominant Species-Physiognomy-Ecological (DSPE) System for the Classification of Plant Ecological Communities from Remote Sensing Images. *Ecologies* **2022**, *3*, 323–335. [[CrossRef](#)]
40. Li, S.; Yan, J.; Liu, X.; Wan, J. Response of vegetation restoration to climate change and human activities in Shaanxi-Gansu-Ningxia Region. *J. Geogr. Sci.* **2013**, *23*, 98–112. [[CrossRef](#)]
41. Akiyama, T.; Kharrazi, A.; Li, J.; Avtar, R. Agricultural water policy reforms in China: A representative look at Zhangye City, Gansu Province, China. *Environ. Monit. Assess.* **2017**, *190*, 9. [[CrossRef](#)] [[PubMed](#)]
42. Zhang, H.; He, Z.; Xu, J.; Mu, W.; Chen, Y.; Wang, G. Analysis of Spatial and Temporal Changes in Vegetation Cover and Driving Forces in the Wuding River Basin, Loess Plateau. *Forests* **2024**, *15*, 82. [[CrossRef](#)]
43. Liu, C.; Zhang, X.; Wang, T.; Chen, G.; Zhu, K.; Wang, Q.; Wang, J. Detection of vegetation coverage changes in the Yellow River Basin from 2003 to 2020. *Ecol. Indic.* **2022**, *138*, 108818. [[CrossRef](#)]
44. Ma, L.; Bo, J.; Li, X.; Fang, F.; Cheng, W. Identifying key landscape pattern indices influencing the ecological security of inland river basin: The middle and lower reaches of Shule River Basin as an example. *Sci. Total Environ.* **2019**, *674*, 424–438. [[CrossRef](#)] [[PubMed](#)]
45. Funk, C.; Peterson, P.; Landsfeld, M.; Pedreros, D.; Verdin, J.; Shukla, S.; Husak, G.; Rowland, J.; Harrison, L.; Hoell, A.; et al. The climate hazards infrared precipitation with stations—A new environmental record for monitoring extremes. *Sci. Data* **2015**, *2*, 150066. [[CrossRef](#)] [[PubMed](#)]

46. Ermida, S.L.; Soares, P.; Mantas, V.; Göttsche, F.-M.; Trigo, I.F. Google Earth Engine Open-Source Code for Land Surface Temperature Estimation from the Landsat Series. *Remote Sens.* **2020**, *12*, 1471. [[CrossRef](#)]
47. Luo, D.; Jin, H.; Wu, Q.; Bense, V.F.; He, R.; Ma, Q.; Gao, S.; Jin, X.; Lu, L. Thermal regime of warm-dry permafrost in relation to ground surface temperature in the Source Areas of the Yangtze and Yellow rivers on the Qinghai-Tibet Plateau, SW China. *Sci. Total Environ.* **2018**, *618*, 1033–1045. [[CrossRef](#)] [[PubMed](#)]
48. Pekel, J.F.; Cottam, A.; Gorelick, N.; Belward, A.S. High-resolution mapping of global surface water and its long-term changes. *Nature* **2016**, *540*, 418–422. [[CrossRef](#)] [[PubMed](#)]
49. Xia, C.; Liu, G.; Zhou, J.; Meng, Y.; Chen, K.; Gu, P.; Yang, M.; Huang, X.; Mei, J. Revealing the impact of water conservancy projects and urbanization on hydrological cycle based on the distribution of hydrogen and oxygen isotopes in water. *Environ. Sci. Pollut. Res. Int.* **2021**, *28*, 40160–40177. [[CrossRef](#)] [[PubMed](#)]
50. Liang, W.; Quan, Q.; Wu, B.; Mo, S. Response of Vegetation Dynamics in the Three-North Region of China to Climate and Human Activities from 1982 to 2018. *Sustainability* **2023**, *15*, 3073. [[CrossRef](#)]
51. Carlson, T.N.; Ripley, D.A. On the relation between NDVI, fractional vegetation cover, and leaf area index. *Remote Sens. Environ.* **1997**, *62*, 241–252. [[CrossRef](#)]
52. Wang, Y.; Zhang, J.; Tong, S.; Guo, E. Monitoring the trends of aeolian desertified lands based on time-series remote sensing data in the Horqin Sandy Land, China. *Catena* **2017**, *157*, 286–298. [[CrossRef](#)]
53. Xu, X.; Liu, H.; Jiao, F.; Gong, H.; Lin, Z. Time-varying trends of vegetation change and their driving forces during 1981–2016 along the silk road economic belt. *Catena* **2020**, *195*, 104796. [[CrossRef](#)]
54. Zhang, Y.; Zhang, C.; Wang, Z.; Chen, Y.; Gang, C.; An, R.; Li, J. Vegetation dynamics and its driving forces from climate change and human activities in the Three-River Source Region, China from 1982 to 2012. *Sci. Total Environ.* **2016**, *563–564*, 210–220. [[CrossRef](#)] [[PubMed](#)]
55. Zhang, D.; Ge, W.; Zhang, Y. Evaluating the vegetation restoration sustainability of ecological projects: A case study of Wuqi County in China. *J. Clean. Prod.* **2020**, *264*, 121751. [[CrossRef](#)]
56. Hou, W.; Gao, J.; Wu, S.; Dai, E. Interannual Variations in Growing-Season NDVI and Its Correlation with Climate Variables in the Southwestern Karst Region of China. *Remote Sens.* **2015**, *7*, 11105–11124. [[CrossRef](#)]
57. Yin, L.; Wang, X.; Feng, X.; Fu, B.; Chen, Y. A comparison of SSEBop-Model-Based evapotranspiration with eight evapotranspiration products in the Yellow River Basin, China. *Remote Sens.* **2020**, *12*, 2528. [[CrossRef](#)]
58. Yin, L.; Feng, X.; Fu, B.; Chen, Y.; Wang, X.; Tao, F. Irrigation water consumption of irrigated cropland and its dominant factor in China from 1982 to 2015. *Adv. Water Resour.* **2020**, *143*, 103661. [[CrossRef](#)]
59. Yang, S.; Liu, J.; Wang, C.; Zhang, T.; Dong, X.; Liu, Y. Vegetation dynamics influenced by climate change and human activities in the Hanjiang River Basin, central China. *Ecol. Indic.* **2022**, *145*, 109586. [[CrossRef](#)]
60. Ma, Y.; Wang, W.; Jin, S.; Li, H.; Liu, B.; Gong, W.; Fan, R.; Li, H. Spatiotemporal variation of LAI in different vegetation types and its response to climate change in China from 2001 to 2020. *Ecol. Indic.* **2023**, *156*, 111101. [[CrossRef](#)]
61. Wang, N.; Du, Y.; Liang, F.; Wang, H.; Yi, J. The spatiotemporal response of China's vegetation greenness to human socio-economic activities. *J. Environ. Manag.* **2022**, *305*, 114304. [[CrossRef](#)]
62. Gu, Y.; Pang, B.; Qiao, X.; Xu, D.; Li, W.; Yan, Y.; Dou, H.; Ao, W.; Wang, W.; Zou, C.; et al. Vegetation dynamics in response to climate change and human activities in the Hulun Lake basin from 1981 to 2019. *Ecol. Indic.* **2022**, *136*, 108700. [[CrossRef](#)]
63. Peng, J.; Jiang, H.; Liu, Q.; Green, S.M.; Quine, T.A.; Liu, H.; Qiu, S.; Liu, Y.; Meersmans, J. Human activity vs. climate change: Distinguishing dominant drivers on LAI dynamics in karst region of southwest China. *Sci. Total Environ.* **2021**, *769*, 144297. [[CrossRef](#)]
64. Ibsch, P.L.; Hoffmann, M.T.; Kreft, S.; Pe'er, G.; Kati, V.; Biber-Freudenberger, L.; DellaSala, D.A.; Vale, M.M.; Hobson, P.R.; Selva, N. A global map of roadless areas and their conservation status. *Science* **2016**, *354*, 1423–1427. [[CrossRef](#)] [[PubMed](#)]
65. Ge, W.; Deng, L.; Wang, F.; Han, J. Quantifying the contributions of human activities and climate change to vegetation net primary productivity dynamics in China from 2001 to 2016. *Sci. Total Environ.* **2021**, *773*, 145648. [[CrossRef](#)]
66. Chen, X.; Guan, T.; Zhang, J.; Liu, Y.; Jin, J.; Liu, C.; Wang, G.; Bao, Z. Identifying and Predicting the Responses of Multi-Altitude Vegetation to Climate Change in the Alpine Zone. *Forests* **2024**, *15*, 308. [[CrossRef](#)]
67. Ma, M.; Zhang, H.; Qin, J.; Liu, Y.; Wu, B.; Su, X. Analysis of Factors Driving Subtropical Forest Phenology Differentiation, Considering Temperature and Precipitation Time-Lag Effects: A Case Study of Fujian Province. *Forests* **2024**, *15*, 334. [[CrossRef](#)]
68. Lin, N.; Li, J.; Jiang, R.; Li, X.; Liu, S. Quantifying the Spatiotemporal Variation of NPP of Different Land Cover Types and the Contribution of Its Associated Factors in the Songnen Plain. *Forests* **2023**, *14*, 1841. [[CrossRef](#)]
69. Lai, J.; Zhao, T.; Qi, S. Spatiotemporal Variation in Vegetation and Its Driving Mechanisms in the Southwest Alpine Canyon Area of China. *Forests* **2023**, *14*, 2357. [[CrossRef](#)]
70. Liu, L.; Zhang, X.; Gao, Y.; Chen, X.; Shuai, X.; Mi, J. Finer-Resolution Mapping of Global Land Cover: Recent Developments, Consistency Analysis, and Prospects. *J. Remote Sens.* **2021**, *2021*, 5289697. [[CrossRef](#)]
71. Gao, Y.; Liu, Z.; Li, R.; Shi, Z. Long-Term Impact of China's Returning Farmland to Forest Program on Rural Economic Development. *Sustainability* **2020**, *12*, 1492. [[CrossRef](#)]

- 
72. Li, Z.; Sun, X.; Huang, Z.; Zhang, X.; Wang, Z.; Li, S.; Zheng, W.; Zhai, B. Changes in nutrient balance, environmental effects, and green development after returning farmland to forests: A case study in Ningxia, China. *Sci. Total Environ.* **2020**, *735*, 139370. [[CrossRef](#)] [[PubMed](#)]
  73. Zhang, X.; Liu, L.; Wu, C.; Chen, X.; Gao, Y.; Xie, S.; Zhang, B. Development of a global 30 m impervious surface map using multisource and multitemporal remote sensing datasets with the Google Earth Engine platform. *Earth Syst. Sci. Data* **2020**, *12*, 1625–1648. [[CrossRef](#)]

**Disclaimer/Publisher’s Note:** The statements, opinions and data contained in all publications are solely those of the individual author(s) and contributor(s) and not of MDPI and/or the editor(s). MDPI and/or the editor(s) disclaim responsibility for any injury to people or property resulting from any ideas, methods, instructions or products referred to in the content.